OPTICA

Computational imaging with meta-optics

Johannes E. Fröch,[1] Shane Colburn,[1] David J. Brady,[2] Felix Heide,[3] Ashok Veeraraghavan,[4] and Arka Majumdar[1,5,*]

[1]Electrical and Computer Engineering, University of Washington, Seattle, Washington 98195, USA
[2]College of Optical Sciences, University of Arizona, Tucson, Arizona 85721, USA
[3]Computer Science, Princeton University, Princeton, New Jersey 08544, USA
[4]Electrical and Computer Engineering, Rice University, Houston, Texas 77005, USA
[5]Physics Department, University of Washington, Seattle, Washington 98195, USA
*arka@uw.edu

Received 28 October 2024; revised 24 February 2025; accepted 17 April 2025; published 30 May 2025

Sub-wavelength diffractive meta-optics have emerged as a versatile platform to manipulate light fields at will, due to their ultra-small form factor and flexible multifunctionalities. However, miniaturization and multimodality are typically compromised by a reduction in imaging performance; thus, meta-optics often yield lower resolution and stronger aberration compared to traditional refractive optics. Concurrently, computational approaches have become popular to improve the image quality of traditional cameras and exceed limitations posed by refractive lenses. This in turn often comes at the expense of higher power and latency, and such systems are typically limited by the availability of certain refractive optics. Limitations in both fields have thus sparked cross-disciplinary efforts to not only overcome these roadblocks but also to go beyond and provide synergistic meta-optical–digital solutions that surpass the potential of the individual components. For instance, an application-specific meta-optical frontend can preprocess the light field of a scene and focus it onto the sensor with a desired encoding, which can either ease the computational load on the digital backend or can intentionally alleviate certain meta-optical aberrations. In this review, we introduce the fundamentals, summarize the development of meta-optical computational imaging, focus on latest advancements that redefine the current state of the art, and give a perspective on research directions that leverage the full potential of sub-wavelength photonic platforms in imaging and sensing applications. The current advancement of meta-optics and recent investments by foundries and technology partners have the potential to provide synergistic future solutions for highly efficient, compact, and low-power imaging systems.

https://doi.org/10.1364/OPTICA.546382

1. INTRODUCTION

The rapid advent of the Internet of Things, wearable technologies, and autonomous navigation systems has accelerated the demand for low-power, low-latency imagers with ultra-compact form factors [1]. A similar need exists for biomedical instruments, where reductions in system volume are critical to reach clinically significant targets inside the body [2,3]. Despite the demand for compact cameras in next-generation technologies, current solutions still rely on century-old optical designs based on refractive components. However, these are often insufficient for emerging applications. While reductions in size, weight, and volume are possible using Fresnel lenses, multilevel diffractive, or binary optics, these concepts exhibit significant aberrations and/or generate multiple diffracted orders, decreasing their overall efficiency. These limitations have fortified a sentiment in the photonics community that diffractive optics are essentially nonimaging optics and limited their utility to niche applications, such as aberration correction in conjunction with refractive optics [4]. By countering these shortcomings of diffractive optics, meta-optics have garnered substantial attention within the research community over recent years [5]. These are sub-wavelength diffractive components, which ensure that all diffracted light is concentrated in the zeroth order, while higher-order diffracted beams are evanescent. Meta-optics are composed of nano- to micron-scale scatterers, which impart different phase shifts on the incident wavefront depending on their geometry and orientation. This enables fabrication with a single lithography stage, significantly reducing the number of masks in the fabrication process. The sub-wavelength periodicity also provides an extremely large space-bandwidth product, and consequently, an extremely large number of degrees of freedom for designing optics. Hence, researchers tout the benefit of meta-optics to achieve multifunctionality, including controlling the polarization and spectrum of light. Finally, the small volume of meta-optics and enhanced light–matter interaction via resonant effects offer an important opportunity to create reconfigurable optics with low-power and higher-speed operation compared to existing free-space reconfigurable optics. While the benefits were known for a long time, and several works existed at least two decades ago [6,7], the

interest in meta-optics has reemerged in recent years for two primary reasons: 1) the availability of sophisticated nanofabrication facilities, including semiconductor foundries, and 2) the ubiquity of computational resources and electromagnetic simulators to design meta-optics. Despite this burgeoning interest and numerous demonstrations of their versatility, their performance remains inferior to state-of-the-art imaging systems that use refractive lenses, even after a decade of renewed research.

While meta-optic concepts have largely been spearheaded by optical scientists and engineers, a parallel effort to reduce the size of imaging systems is happening in the computer science community. With the ubiquity of image sensors in consumer electronics, along with the availability of powerful computing resources in almost all imaging devices, there is a unique opportunity to enhance image quality via computation [8]. By using computational imaging [9], researchers have drastically miniaturized complex imaging systems by replacing sophisticated compound optics with simple lenses [10,11] and leveraged software to mitigate aberrations [12–15]. Although this started with simple linear deconvolution and denoising routines, in recent years, there has been a growth in learned reconstruction techniques and artificial neural networks (ANNs) to enhance imaging performance. Unfortunately, computational reconstruction algorithms typically increase power consumption and latency, which may render them unsuitable for power-constrained, real-time applications. Additionally, many tasks in machine vision applications only require specific features or subregions of a frame for inference [16]; thus, only a section or a downsampled version of the full image is necessary to support digital feature extraction [17]. Beyond that, many applications require information embedded in other light-field parameters (e.g., polarization, spectrum, and incidence angle), which may require significant computation or can only be applied within specific scenarios [18–23].

While a large body of research exists on both meta-optics and computational imaging [24], these two fields have remained largely separated, and only very recently, their synergistic effects become apparent. Largely fueled by the desire to exceed limitations in both domains, researchers have devised architectures for partitioning the imaging process into both the optical and digital realms (Fig. 1). In this mini review, we first provide a brief tutorial on both meta-optics and computational imaging. We then discuss the current state of meta-optics-based computational imaging. Although still in its infancy, the combination of meta-optics with computational imaging has already resulted in imaging performance surpassing expectations of image quality with diffractive optics. Finally, we discuss several promising future research directions, where the advantages of meta-optics and computational imaging can be further exploited. As such, in our opinion, the exploration of multifunctionality and hardware-software co-optimization will constitute two key future research directions in the field of meta-optics.

2. BASICS OF META-OPTICS AND COMPUTATIONAL IMAGING

We will start with a brief tutorial on the fundamentals of meta-optics design and computational imaging. A primer on the fabrication and characterization of meta-optics is in Supplement 1. While in recent years, there are several papers highlighting the difference between meta-optics and traditional diffractive optics [25,26]; in our opinion, meta-optics is just a special class of sub-wavelength diffractive optics. In practice, by going to sub-wavelength features, a meta-optic can implement a higher phase gradient and thus offers a more diverse platform for various phase functions compared to their coarser-pitch, super-wavelength diffractive counterparts. The sub-wavelength periodicity also allows controlling the phase via lateral geometry of the scatterers, allowing single-stage lithography to fabricate the meta-optics. Finally, the small periodicity mitigates higher-order diffraction compared to traditional diffractive optics and can potentially provide higher efficiency and less spurious light when multiple optics are cascaded [27].

A. Computational Design of Meta-Optics

Meta-optics pose a tremendous multiscale electromagnetic design challenge. Due to their sub-wavelength feature size, capturing their response accurately requires a full-wave simulation, such

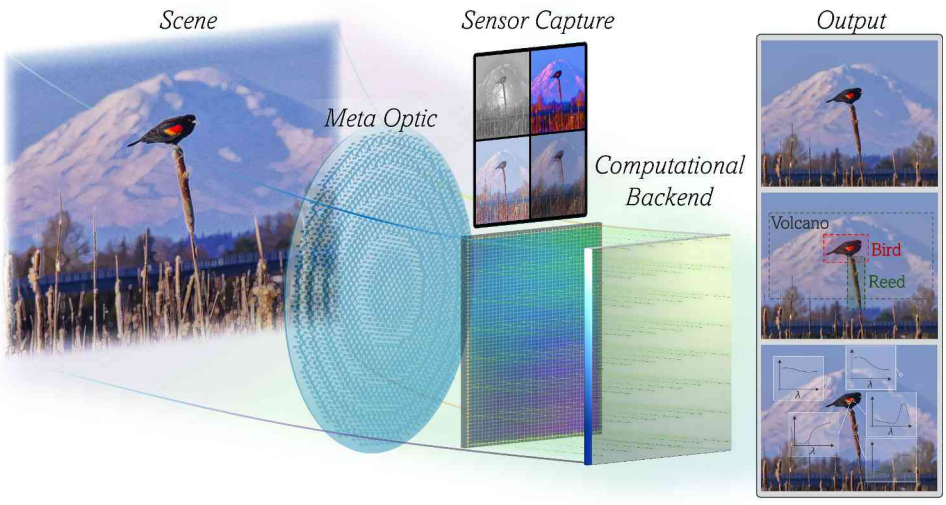

Fig. 1. A synergistic combination of meta-optics (hardware) and digital computational backend (software) can result in imaging performance, not achievable with pure optics and computational imaging alone. Current research in this field has primarily been focused on high-quality imaging, multimodal imaging (depth and spectral sensing), and object detection.

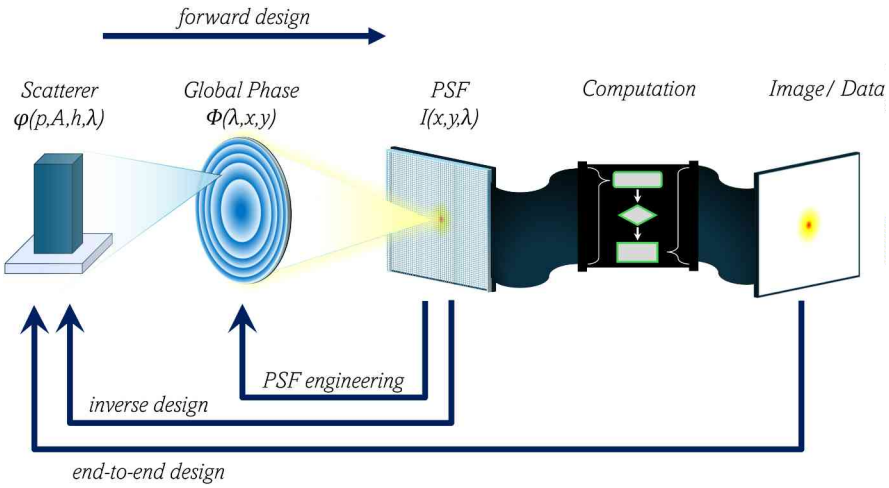

Fig. 2. Design paradigm of meta-optical computational imaging systems: via full-wave simulation of the sub-wavelength meta-atoms, we can abstract out the scatterers as a phase mask. This allows simulating a large aperture meta-optics and calculate the PSF, which is then passed to a computational block. At different abstraction levels (either scatterers or phase mask or after computational block), we can perform inverse design of the meta-optical computational imaging system.

as a finite-difference time-domain (FDTD) method or rigorous coupled-wave analysis (RCWA) [28]. However, their large aperture size on the order of $\sim 10^3-10^4\lambda$ (λ is the optical wavelength) makes such methods impractical. Thus, ray or wave optical methods are typically employed. In Fig. 2, we outline typical design approaches to illustrate common challenges, starting at the left end with the elemental scatterers (meta-atoms), which impart a complex phase on the impinging wavefront. By arranging scatterers of various sizes and shapes, a global phase profile is implemented, which generates a point spread function (PSF) for the transmitted (reflected) light. The absolute Fourier transform of the PSF provides the modulation transfer function (MTF), which indicates that the contrast at certain spatial frequencies is preserved as the scene is captured with the optical system and sensor. At the other end of this design framework, we can consider the sensor and a computational backend, which allow us to leverage computational postprocessing algorithms to reconstruct a final image or extract data beyond simple image captures.

In forward design, the phase and amplitude response of the scatterer are first calculated and then mapped to a global phase profile that is given by a closed-form expression or based on intuition. The most common analytical functions for lenses are those of a hyperboloid [29–32], square [33–35], extended depth of focus (EDOF) [36,37], and vortex profiles [38–40]. Up to a certain degree, the functionality of the system can be expanded by combining multiple phase masks, enabling spectroscopy [41–43], polarization imaging [44,45], Moiré lenses [46–48], Alvarez lenses [49,50], and depth-sensitive imaging [51–53]. A common assumption made is the locally periodic (phase) approximate (LPA), whereas coupling between neighboring dissimilar scatterers is considered negligible [54]. Empirically, this approximation works well for smoothly varying, low-gradient phase profiles, while for structural discontinuities and rapid variation, strong wavefront distortion and undesired scattering may occur [55–58]. This is primarily because, with a rapidly varying phase, the neighboring scatterers are more dissimilar, weakening the locally periodic approximation. Another aspect that should be considered is the sampling rate for the implementation of the phase profile, which can limit the implementable phase gradient among neighboring scatterers or even lead to undesired aliasing effects [59,60]. A caveat of forward design approaches is their limitation to a single or few wavelengths [61,62], as phase wrapping induces chromatic aberrations [61,63]. To counteract this, dispersion engineering approaches have been developed, where an essentially larger variation in the scatterer geometry yields a larger phase diversity to satisfy the phase conditions for multiple wavelengths simultaneously [64–71]. However, this approach is fundamentally limited to small Fresnel numbers (small numerical aperture and/or small aperture) [72].

To expand the landscape of device functionalities, the design methodology can be reversed, which allows functionalities that are not intuitively known. We can define a custom figure of merit, or an intensity distribution/PSF, and then obtain the scatterer distribution that will generate this response [73]. Somewhere in between forward and inverse design methods fall approaches where a global phase profile is derived inversely (e.g., through ray-tracing or phase-retrieval algorithms, such as the Gerchberg–Saxton method [74]), and scatterers are mapped to that global phase profile, as often used for meta-optic holography. These approaches are particularly powerful for single-wavelength applications, where in a subsequent step, a scatterer library can be readily mapped onto that specific derived phase profile. However, for broadband or polychromatic applications, this methodology suffers from the same limitations as forward design approaches.

The crux of inverse design approaches for broadband and polychromatic operation is the requirement of a differentiable relation between the structural parameters of scatterers and the corresponding phase shift, which accurately incorporates the scatterer dispersion. There are several other methods, such as genetic algorithms, which do not require differentiability; however, differentiability helps with efficient optimization and is also more amenable to end-to-end design. Due to the sub-wavelength size, the optical response of the meta-atoms is often governed by resonances, and an analytical or differentiable relation between meta-atoms and the phase cannot be readily established. This problem becomes more severe with complex scatterer shapes, which are expected to provide better functionality. Recent works have overcome this problem by implementing proxy functions or neural networks to make this relationship differentiable [75,76].

Once this function is established, one can consider a full end-to-end design pipeline, where the computational backend and the meta-optics are optimized concurrently. From a system level, this allows to fully leverage and complement strengths and weaknesses of constituent parts.

B. Computational Imaging

Computational imaging encompasses techniques that exploit attributes of the imaging system itself to enhance, augment, or extract additional information from the captured sensor data [9]. The breadth of approaches has enabled various modalities, which utilize various optical elements (or no optical element at all [77–79]), such as common refractive lenses [15,80], diffusers [81], and designed coded phase masks [82]. These optical systems work in tandem with software that can either manipulate/enhance/reconstruct or extract more information. While this field has developed steadily over the last two to three decades, in recent years, there has been significant growth with the development of improved and ubiquitous smartphone cameras, better graphics processing units (GPUs), and the advancement of machine learning (ML)/artificial intelligence (AI). Some examples include the advanced imaging capabilities/modalities available in smartphones, which enable on-the-fly high-quality imaging with ∼10 to 100 megapixel images with low noise, imaging at extremely low light conditions, depth-sensing capabilities, and other exciting developments [8,83].

To give readers intuition regarding this approach, we illustrate a simple strategy to improve image quality using a standard nonblind deconvolution method, Wiener deconvolution, which considers a known PSF. As outlined in Equation 1, an image y is formed as a convolution of a shift-invariant PSF with a ground truth x and additive sensor noise n:

$$y = \mathrm{PSF} \circledast x + n.$$

One approach to deconvolve the image is given using an inverse filter in the Fourier domain, where F describes the Fourier transform, $*$ denotes the complex conjugate, and SNR is the signal-to-noise ratio in the measurement: $\tilde{x} = F^{-1}\left\{\frac{F\{\mathrm{PSF}\}^* \cdot F\{y\}}{|F\{\mathrm{PSF}\}|^2 + \frac{1}{\mathrm{SNR}}}\right\}$. While this approach has been successful, the breadth of deconvolution approaches has increased in recent years, significantly covering inverse filters [15], iterative approaches [81], neural networks [75,84,85], and optics with spatially varying PSFs [86].

Smartphone-based imaging and significant developments in biomedical imaging applications have driven this field to a point where computational imaging has been successfully used for super-resolution microscopy [87,88], depth-sensitive microscopy [89–91], and gigapixel imaging [80,92]. We note that this field is far too extensive to be covered in this section and refer the reader to various extensive reviews from recent years [9].

3. CURRENT STATE OF THE ART OF META-OPTICS-BASED COMPUTATIONAL IMAGING

The field of meta-optical computational imaging is less than a decade old, and its full potential is yet to be explored, as we will discuss later. Current works on meta-optical computational imaging can be broadly classified into three categories: achromatic, large field-of-view imaging; multimodal imaging; and meta-optical encoding to aid computer vision tasks.

A. Achromatic Large Field-of-View Imaging System

The most ubiquitous use of optics is to capture high-quality images. In fact, almost all current consumer electronic devices come with a visible camera, which relies on multiple optical elements to capture high-quality images. A similar need for surveillance, defense, and national security applications necessitates capturing high-quality images in the infrared range. Almost all these applications require broadband imaging with a large field of view and often with large apertures to maximize light collection. The size of the aperture can range from ∼2 mm (for consumer electronics) to ∼50 cm (for defense applications). A common desire is to reduce the size, weight, power, and cost (SWaP-C) of these systems. Given their thinness and the ability to implement high-phase gradients, meta-optics can potentially reduce the thickness of imaging systems. Additionally, their weight does not scale with volume like refractive optics, providing an advantage for large aperture optics. However, it is imperative that the SWaP-C benefit does not come at the cost of degraded imaging performance.

Unfortunately, meta-optics suffer from strong chromatic aberrations. While several works have tried to solve this problem using dispersion engineering [64–66,69,93–95], it is limited to small aperture sizes on the order of 10's of microns for even moderate numerical apertures. This problem can be alleviated using computational imaging. In fact, computational imaging was first used in conjunction with EDOF cubic meta-optics for full-color visible imaging [37]. A traditional hyperboloid metalens focuses light on a diffraction-limited spot for a single wavelength, but the focal length f_{lens} of the lens changes with the optical wavelength λ following $\lambda \times f_{\mathrm{lens}}$ being constant. Thus, for a fixed lens-sensor distance, one wavelength is well focused, while all other wavelengths are strongly defocused. With an EDOF meta-optic, the depth of focus is increased such that even with the associated chromatic focal shit, all wavelengths in the target band reach the sensor in an identical fashion. If the response of the optics is "invertible" (as governed by their MTF), then we can reconstruct the image computationally from the captured scene. An "invertible" response essentially means that the signal-to-noise contrast is large enough that its reciprocal is finite. As such, any optical response will be invertible up to a certain spatial frequency, as the signal contrast will decrease with larger spatial frequencies. Initial works involved cubic phase masks to achieve an EDOF, while later works explored the utility of radially symmetric meta-optics, such as log-asphere phase profiles [36,96]. Limitations, in terms of image quality, ultimately led to the use of inverse design to enable EDOF meta-optics and full-color imaging [97]. While EDOF meta-optics correct for chromatic aberrations, their overall image quality remains relatively poor, with distortions, such as background noise, residual deconvolution artifacts, and uncorrected aberrations at higher field angles [37]. The image quality of single meta-optics improved dramatically with a co-optimized computational backend, which also considered larger field angles [75]. Here, a differentiable pipeline was used to optimize the image quality after considering a computational backend. This work reported high-quality imaging with a 0.5 mm aperture $f/2$ meta-optics [Figs. 3(a) and 3(b)] [75]. A key innovation was a differentiable mapping between meta-atoms and their phase response. While initial works relied on a polynomial mapping, recently deep learning-based approaches have

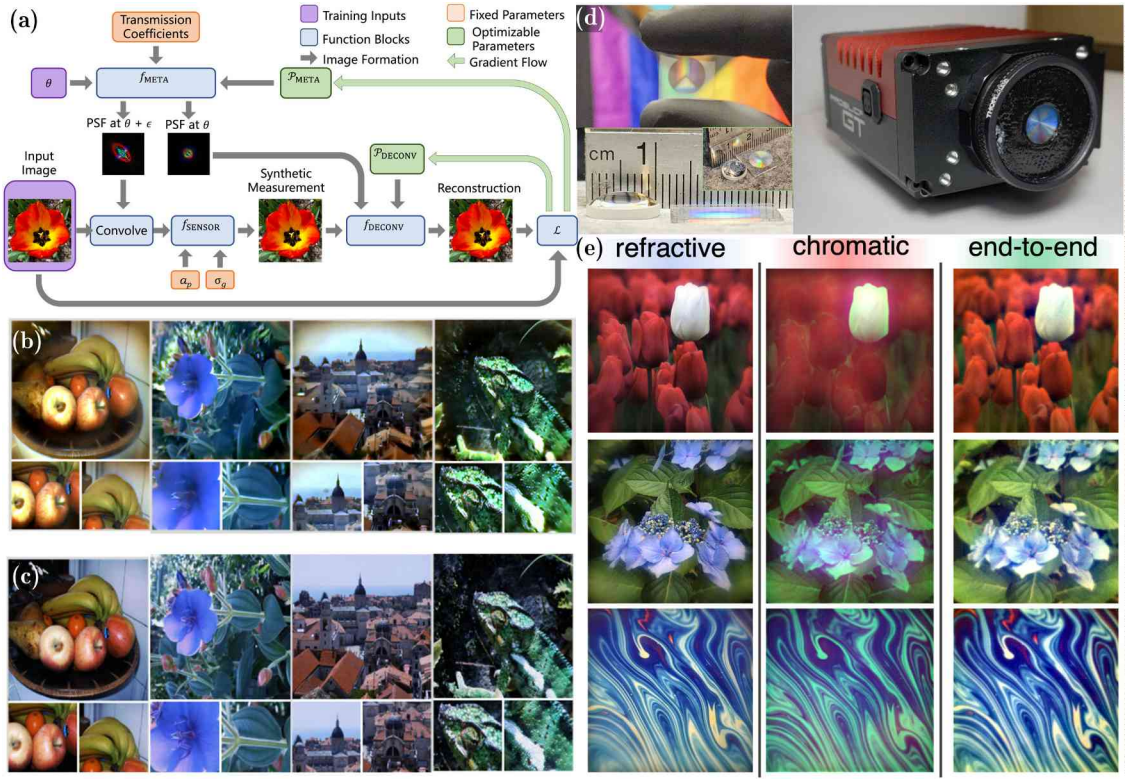

Fig. 3. Full-color imaging exploiting co-designed meta-optics and computational backend: (a) design framework to co-optimize the meta-optic and reconstruction algorithm via a differentiable pipeline. Reproduced with permission from Springer Nature [75]; (b) images captured using a single 500 μm, f/2 meta-optics. Reproduced with permission from Springer Nature [75]; (c) same images captured using a six-element compound optic [75]. (d) Similar design method is used to create 1 cm aperture meta-optics, which can be directly integrated with an image sensor (without relying on a relay optics). Reproduced with permission from Springer Nature [100]. (e) The large aperture allows capturing video rate full-color images using a single end-to-end designed meta-optics with comparable image quality of a refractive optics. Reproduced with permission from Springer Nature [100].

enabled modeling complex scatterer shapes with resonances, which provide larger phase diversity [98,99]. For image reconstruction, several methods, including Wiener deconvolution and neural networks, were employed. For neural network-based approaches, a feature propagator was used to ensure high-quality reconstruction while maintaining generalizability. The feature propagator network was based roughly on a U-Net structure, the early layers of which extracted features at multiple resolution scales. These features were then passed through a filtering step akin to Wiener deconvolution, but rather than acting on the image, the features themselves were filtered, hence the name "Feature Propagator" as the blurred and noisy features were propagated through a filtering operation. The final stages of the network then mirrored the early layers, mapping the filtered features back into a high-resolution image that is deconvolved and denoised. Compared to traditional U-Nets, this architecture is more general, leveraging aspects of more traditional filtering approaches like Wiener deconvolution, while maintaining many of the denoising advantages of a neural network approach, wherein the introduction of nonlinear operations helps to mitigate noise. Recently, a similar end-to-end design framework has been extended to report full-color imaging in the visible using a 1 cm aperture $f/2$ meta-optic with a $\sim 30°$ field of view [Figs. 3(c) and 3(d)] [100]. An extensive characterization of the meta-optic revealed that the end-to-end design preserves high spatial frequency information by trading off the low spatial frequency contrast. Such a trade-off maintains a similar MTF over the full wavelength range of interest, and the reduced contrast can be retrieved computationally. Such a trade-off is similar to what is seen in diffraction-free beam propagation, where the optical beam maintains its shape over an extended depth but at the cost of being more spatially delocalized compared to a diffraction-limited spot. While Wiener deconvolution-based approaches already preserve color information, diffusion neural networks produce image quality comparable to that of a state-of-the-art smartphone camera [100]. Of course, the caveat is that the diffusion network's latency precludes real-time processing at video rates. While end-to-end design demonstrated the efficacy of a co-designed meta-optic with a computational backend, several recent works reported full-color imaging using a hyperboloid metalens (i.e., an analytical phase profile and the lens were not optimized for broadband operation) and a deep learning backend [84,101]. While most broadband meta-optics works primarily focused on the visible wavelength range, recently broadband imaging has been reported in the long-wave infrared regime (8–12 μm) using an all-silicon single meta-optic [98]. Here, only the optics is optimized to increase the volume under the MTF curve, and the computational backend was separately designed.

We emphasize that while computational meta-optics enhance the performance, the image quality remains inferior to that of a compound refractive lens. However, current smartphone lenses consist of ∼8–10 refractive optics, and it is expected that a single surface may not be able to achieve the functionalities of all these. A more promising route would be to use meta-optics as a corrector

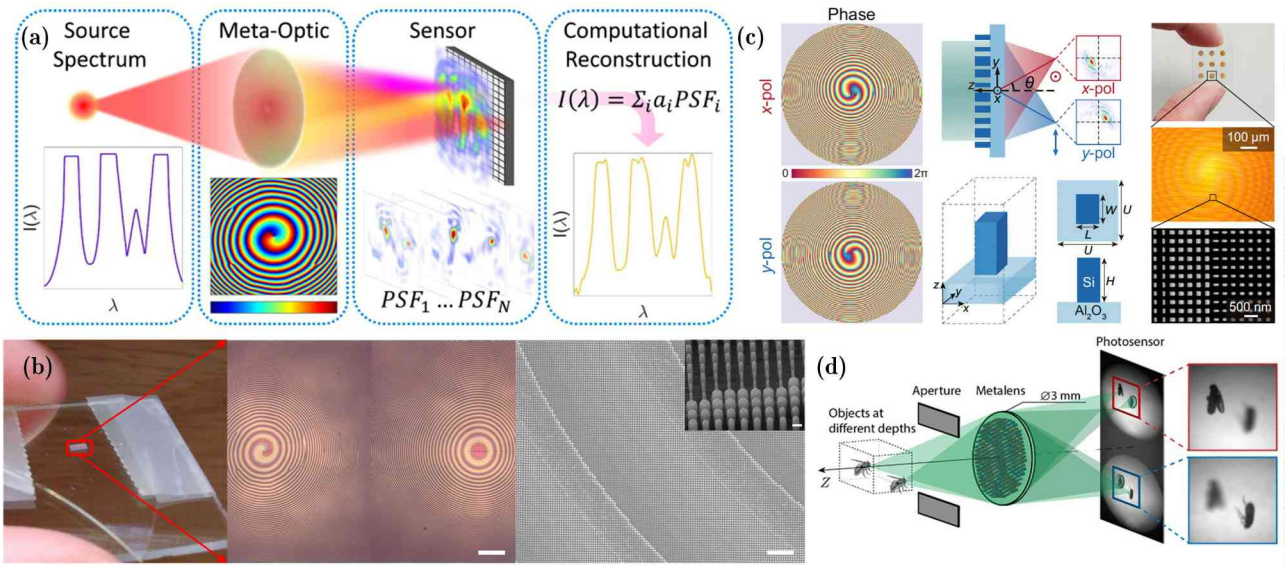

Fig. 4. Multimodal imaging using meta-optics: (a) computational spectroscopy using meta-optics exhibiting wavelength-dependent PSF. Reprinted with permission from Ref. [42]. Copyright 2023 American Chemical Society; (b) using two meta-optics (one with depth-invariant PSF and one with depth-varying PSF) placed on a single surface and computational reconstruction, researchers demonstrated depth sensing. Reprinted with permission from Ref. [51]. Copyright 2020 American Chemical Society; (c) by multiplexing different meta-optics exploiting polarization depth and polarization imaging has been reported. Reprinted with permission from Ref. [52] under a Creative Commons Attribution 4.0 International License [113]; (d) by using two meta-optics (depending on polarization) with different focal lengths, researchers demonstrated depth sensing. Reproduced with permission from Ref. [112]. Copyright 2019 National Academy of Science.

[102] and to combine these with refractive lenses to achieve broadband performance and alleviate aberrations. To that end, a 6 mm hybrid refractive/meta-optic was reported for broadband imaging [103]. Nevertheless, achieving all performance criteria, in terms of field of view, achromatic operation, aberration-free imaging, image size, and pixels per degree, remains elusive thus far. We believe that new innovations and engineering approaches will be required to solve this problem, and as such, more future work will be needed.

B. Multimodal Imaging System

Among other imaging modalities, meta-optics have been used to measure various light-field parameters, such as polarization, spectra, and phase. Several of these works, such as polarimetric imaging with meta-optics [44], however, did not involve a computational approach, and we therefore did not further discuss them in this review. Exploiting the chromaticity of meta-optics, researchers have also reported spectroscopy and hyperspectral imaging [41,104,105]. Notably, with a computational imaging approach, the complexity of the optics can be reduced [106]. For instance, researchers recently demonstrated dual-band spectroscopy, exploiting an engineered, wavelength-dependent PSF [90,91] [Fig. 4(a)]. Rather than having a separate refractive lens or relay in conjunction with a phase mask or spatial light modulator (SLM) that imparts a wavefront coding term, by including a power term in the meta-optic itself, the chromatic focal shift induces a misfocus that in turn rotates two lobes of the PSF. While a phase mask and a separate focusing optic may exhibit similar behavior (this has been used extensively for depth sensing [90,91,107–110]), the effect is more pronounced in a meta-optic owing to its severe chromatic aberration, which can be exploited to improve the sensitivity of a spectrometer design. For an unknown spectrum, a captured image will have the information encoded as a weighted average of different PSFs for each wavelength. By precalibrating the PSFs, the unknown spectrum can then be computationally extracted using techniques, such as Tikhonov regularization [42] or learning-based methods. By using SiN on silicon meta-optics and computational reconstruction, researchers demonstrated spectroscopy with a spectral resolution of ∼3 nm at two different bands centered at 1550 and 1310 nm.

Beyond spectroscopy, meta-optics have also been used for depth sensing. One of the first works in this domain used a meta-optic with a depth-dependent, rotating PSF [51]. In this demonstration, two metasurfaces were used [Fig. 4(b)], one producing a depth-variant PSF, whereas the second meta-optic was depth invariant, enabling reconstruction of both spatial and depth information in an image. A set of corrections to compensate for off-axis aberrations, such as field curvature, was included such that a fractional ranging error close to 1% was maintained over the full field of view. Subsequently, a recent work combined two apertures into a single one, exploiting polarization-dependent scatterers [111]. In another work, a similar polarized scatterer approach was used to multiplex two lenses with different focal lengths in one aperture [Fig. 4(d)], where images at two different depths are captured with a different defocus, enabling computational depth measurement. The combination of polarized multiplexing and a DH-PSF was further used to demonstrate a compact monocular camera equipped with a single-layer metalens that captures 4D images, including 2D all-in-focus intensity, depth, and polarization of a target scene [Fig. 4(c)]. The metalens is optimized to have a conjugate pair of polarization-decoupled rotating single-helix PSFs that are strongly dependent on the depth of the target object. Combined with an image retrieval algorithm, the camera can simultaneously perform high-accuracy depth sensing and high-fidelity polarization imaging over an extended depth of field [52]. The chromatic aberration inherent in a hyperboloid metalens was

also employed for depth sensing, exploiting focusing at different depths for different wavelengths. By collecting images over a large spectral range, one can thus obtain sufficient information to reconstruct depth. This concept, coupled with the transport of intensity equation, has been used to quantitatively estimate phase in an endoscope [114].

Meta-optic arrays have also been used for light-field imaging applications [115]. Holsteen and co-authors utilized an interleaved design to perform single-particle tracking [116]. In that work, laterally separated views of the same scene enable spatial localization of a fluorescent bead. Separately, a 60×60 array of dispersion-engineered meta-optic has also been used to demonstrate depth imaging [115]. While most current works essentially replicate refractive lenslet arrays (and thus suffer from the typical low resolution associated with light-field imaging), metalenses can potentially enable lenslets with overlapping apertures, providing new opportunities.

Computational imaging has been used for varifocal imaging systems, where conventional tuning mechanisms entail moving parts or complex control circuitry. In one example, a cubic metasurface was utilized in combination with a deconvolution routine for depth-invariant imaging exceeding 1 cm at a high numerical aperture [117]. The cubic metasurface provides a depth-invariant PSF, which allows imaging at different object and image distances in a finite conjugate system. Due to the sub-wavelength periodicity, such varifocal imaging can be performed while maintaining a large numerical aperture.

C. Meta-Optical Encoder

In the photonics community, there has been significant interest in optical neural networks in the past decade, while one of the most important and challenging problems in computer vision is detecting and identifying objects within a scene. Although these systems have shown promising results [118–120], they have been severely limited from a system's perspective in terms of practicality for low-power, low-latency processing of data from real-world scenes under ambient illumination.

An alternative approach to most photonic neural networks relies on using a meta-optic as a preprocessing component, an optical frontend, that performs computation before converting intensity signals into the electronic domain for subsequent processing [120,121]. This approach by contrast has the potential to provide a true photonic advantage for optical neural networks from a system's perspective when considering latency and power. Current efforts in designing meta-optical frontends can be broadly classified in two categories: arbitrary vector–matrix multiplication using multiple optics and PSF engineering to perform convolution using a single optic. In both cases, the performance benefit at a system level remains questionable, as benchmarking with existing GPU-based inference shows little benefit in terms of latency and power to implement only the first layer [121]. One possible avenue to improve this is to implement multiple linear layers with optics by taking the information back and forth between the optics (for linear operation) and the digital domain (for nonlinear operation). However, the large latency and power associated with signal transduction (in display and image sensors) render such a hybrid approach sub-optimal. Transferring a large number of linear operations to the frontend by implementing them in optics and then performing digital operations can provide a benefit, though. We emphasize that pure linear operations can also provide some classification in simple systems, e.g., the handwritten dataset in MNIST is linearly separable, and researchers have demonstrated classification with only linear operations using multilayer diffractive optics [122].

To understand the efficacy of a meta-optical frontend, a recent work performed an end-to-end design of a hybrid meta-optics/digital neural network [123]. Their experimental framework quantified the energy and latency of the network by the input dimension being passed to the digital backend [Fig. 5(a)]. An empirical finding from this work is that an optical frontend can be beneficial for computer vision when the latency and power are both highly constrained. However, such an advantage is achieved when the overall accuracy is lower than what can be obtained using the best-trained digital ANN. By using an end-to-end designed meta-optical frontend, researchers recently demonstrated high classification accuracy with the CIFAR-10 dataset [124]. While a purely digital version needs 57M parameters (with a classification accuracy of ∼72.64%), a hybrid optical–digital version requires only 2K parameters while maintaining a similar classification accuracy (∼73.80%). Here, the end-to-end design exploits the spatially varying PSF of the meta-optics, which is considered a limitation of meta-optics for imaging.

While end-to-end design can potentially provide the best possible performance and an optimal load distribution between an optical frontend and a digital backend, such a design requires significant computational resources to model the meta-optic. A simpler solution would be to train the network using a traditional digital pipeline and then implement specific digital operations using optics. By identifying that under incoherent illumination, the formed image is a convolution between the object and the incoherent PSF of the optics; we can pose the convolution as a PSF engineering problem. However, an incoherent PSF is always positive, but a convolution in an ANN generally has both positive and negative values in the associated kernels. We can mitigate this problem by separating the convolution kernel into positive and negative parts and then digitally subtracting the separate convolutions. Such a dual-pupil synthesis approach had been employed in the past [125], but the noise from the two separate apertures is additive when the convolutions are subtracted, complicating already existing challenges with the overall signal-to-noise ratio. Fortunately, by exploiting a digital backend more robust to noise, such a dual-pupil synthesis approach can work for meta-optical encoding. However, translating a single convolution layer from the digital to the optical domain does not provide enough benefit in terms of power and latency. To circumvent that, researchers reported a knowledge distillation-inspired training algorithm, which allows effectively removing some of the nonlinear layers to create a single linear convolution operation that effectively implements multiple linear layers of an ANN [126]. Using such a method, researchers recently reported a compressed meta-optical frontend that allowed at least four orders of magnitude reduction in the operations while suffering a classification accuracy reduction of only 3% for the MNIST dataset [Figs. 5(b) and 5(c)]. While this work implements only one color, exploiting the chromaticity of the meta-optics, one can implement three different kernels for three different meta-optics to further increase the information processing capability of the meta-optics [Fig. 5(d)] [129]. Another way to perform convolution is to employ two meta-optics [Fig. 5(e)] [120,131]: one of them acts as a lenslet array (implemented using

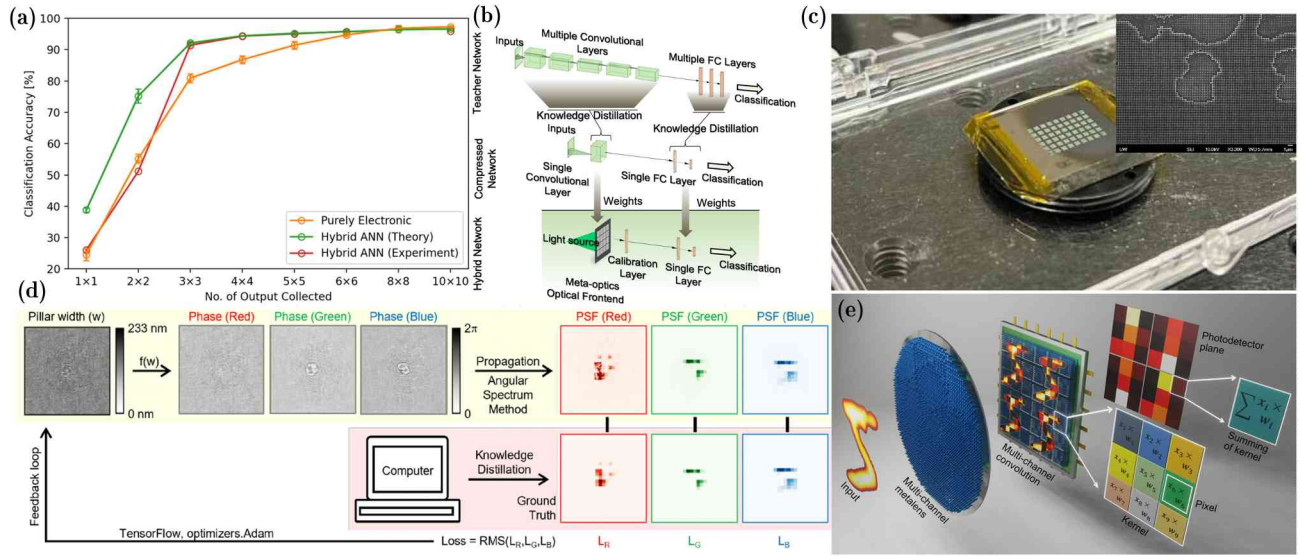

Fig. 5. Meta-optical encoder: (a) by end-to-end designing a single meta-optic and computational backend, a regime for photonic advantage has been identified. While photonic frontend can provide higher classification accuracy as we pass less data to the computational backend (which lowers the latency and power), the overall classification accuracy in this advantageous regime turned out to be lower. Reprinted with permission from Ref. [123] under a Creative Commons Attribution 4.0 International License ([113]). (b) By knowledge distillation, multiple convolutional layers can be collapsed into one convolutional layer, which can be implemented using meta-optics. The meta-optics is designed (via holographic technique) to have a PSF that matches the spatial shape of the desired kernel. Reproduced with permission from Ref. [127] under a Creative Commons Attribution 4.0 International License ([113]). (c) Multiple convolution operations can be performed in parallel using spatially separated meta-optics. The use of only single metasurface drastically reduces the complexity of the optical frontend. Reprinted with permission from Ref. [128]. (d) Exploiting inherent chromaticity of the meta-optics, different convolution operations can be realized for different colors using a single meta-optics. Such capability can implement multichannel convolution and perfectly suited for real-world imaging. Reproduced from Ref. [130]. (e) Instead of a single meta-optics, the convolution operation can be realized using two meta-optics: one creating multiple copies of the image and one implementing the matrix. Reproduced with permission from Ref. [131].

multiplexed meta-atoms, such as polarization-selective meta-atoms), which creates multiple copies of an image. The second meta-optics has the necessary matrix element. When the second meta-optic is placed at the image plane of the first meta-optic, one can perform the necessary vector–matrix multiplication. While such an approach can potentially provide more accurate convolutional operations, the use of two meta-optics may increase the alignment and packaging complexity.

4. CHALLENGES AND OPPORTUNITIES: FUTURE RESEARCH DIRECTIONS

A. Programmable Meta-Optics

Reconfigurable meta-optics can offer complex functionalities unachievable with static optics, overcoming some of the trade-offs in multimodal imaging. For example, instead of achieving both a large field of view and full-color imaging in a single static aperture, an achromatic lens could scan across the whole field of view. Such reconfiguration could also help to collect different parameterized images at different times and yield high-resolution multimodal images. Even for encoding, a reconfigurable frontend can increase the information processing density. Especially, more complex ANN architectures, such as vision transformers [132], will require a dynamic frontend.

Given the high potential and need, various works on tunable meta-optics have already demonstrated their large potential [133,134]. High-speed free-space modulation has been reported using free-carrier effects in degenerately doped semiconductors [135,136] and organic electro-optic polymers [137]. Many of these works touted the possibility of creating a large space-temporal bandwidth product (product of the number of pixels and refresh rate of the phase plate signifying the number of optical beams being tuned in unit time) over state-of-the-art SLMs based on liquid crystal or micro-electro-mechanical systems (MEMS). While LC and MEMS systems are indeed slow, the current limitation of space-temporal bandwidth product ($\sim 10^9$) primarily comes from electronic control, and as such it is unlikely to improve without significant progress in co-packaged electronics and photonics [138]. We emphasize that, while large-scale electronic control is routine in display applications, to achieve $\sim$ MHz $-$ GHz modulation per pixel will require fundamental innovations in co-packaging electronic integrated circuits and photonics. This problem is exacerbated by the need to modulate a large number of pixels, posing a serious problem for routing both electronic and photonic signals [137]. Additionally, feeding in a large amount of data, as is imperative for the large space-temporal bandwidth product SLM, will be extremely power hungry. We believe that instead of a large modulation speed, a large effective change in index is more desirable to tune the meta-optical frontend in most emerging applications. Especially for imaging or encoding applications under ambient light, the speed of operations is often limited to $\sim$kHz. However, in each iteration, a completely new phase mask is needed, and simple global tuning of meta-optics is not sufficient. To that end, in our opinion, the conventional techniques of liquid crystal and MEMS are still very powerful, and combining them with meta-optics can provide the added advantage of energy efficiency and higher speed due to the small feature size. For example, in current liquid crystal-based SLMs, the speed is limited due to the large volume of each pixel. We need a long propagation length to ensure the full 2π

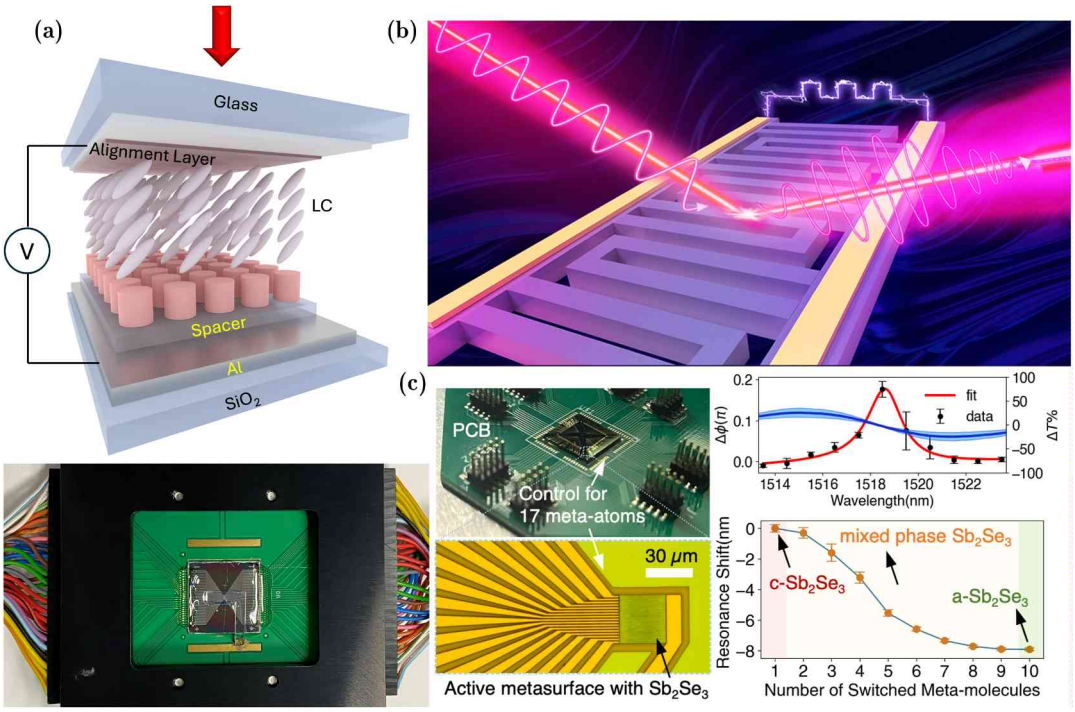

Fig. 6. Reconfigurable meta-optics: (a) by integrating liquid crystal with meta-optics, researchers demonstrated independent control of 96 meta-atoms. Reprinted with permission from Ref. [143]. Copyright 2023 American Chemical Society; (b) independently controlled 1D SLM using nanomechanical meta-optics. Reprinted with permission from Ref. [144]. Copyright 2021 American Chemical Society; (c) by integrating wide bandgap phase-change material Sb_2Se_3, a rudimentary 1D SLM with 17 elements have been reported. Reprinted with permission from Ref. [152]. Copyright 2024 American Chemical Society. All these structures exploit resonances, and the operating optical bandwidth is low.

phase shift. The lateral size of the pixels is then limited by the thickness to minimize cross talk between pixels. By exploiting the local resonances in meta-atoms, the required thickness can be significantly reduced, which in turn helps reduce the lateral dimension of the liquid crystal pixels. This increases the spatial-bandwidth product (due to sub-wavelength periodicity) and the energy to control each pixel. Similarly, the ultra-thin and lightweight nature of the meta-optics is key to enabling mechanical tuning with low energy. In fact, several groups have already reported tunable meta-optics using liquid crystal [139] and MEMS [140–142]. Specifically, in recent work, researchers demonstrated independent tuning of 96 meta-atoms integrated with liquid crystal [Fig. 6(a)] [143]. For any practical applications, however, we need a much larger number of control signals, and a tight collaboration between electronics and optics will be needed. For MEMS, most of the reported works have so far been limited to globally tunable varifocal lenses and rudimentary independent control of 1D meta-optics [Fig. 6(b)] [144]. While a 2D MEMS-based SLM is very similar to grating light valve technology [145], the scaling of each element to the sub-wavelength scale can provide higher energy efficiency, albeit this will significantly increase the complexity of routing and control circuits. Another promising direction for programmable meta-optics is to employ chalcogenide-based phase-change materials (PCMs), which exhibit a large nonvolatile change in refractive index ($\Delta n \sim 0.7$–1) under phase transition [146–148]. PCMs have also been integrated with meta-optics for free-space modulation of light [149–151]. One intriguing aspect of PCMs is their nonvolatile tuning, which has in-built memory in the reconfiguration process and thus can significantly reduce the control complexity for independent tuning of a large number of pixels in a spatial light modulator. Recently, a primitive 1D SLM with PCM Sb_2S_3 has been demonstrated with independent control of 17 meta-atoms [Fig. 6(c)] [152]. Here, a guided mode and bound state in continuum resonance were used to enhance the effective phase shift from Sb_2S_3, and a quasi-continuously tunable notch filter has been reported. As such, scaling the number of pixels and controlling a 2D array of meta-atoms remain an outstanding challenge, solving which can dramatically enhance meta-optical computational imaging systems. An additional challenge for a PCM-based SLM is the reconfiguration mechanism which is current driven, unlike MEMS or liquid crystals (which are field driven), and requires high power consumption during switching.

B. Synthetic Aperture Imaging

Conventional lens-based imaging systems face stringent trade-offs between light throughput, resolution, depth of field, and size (volume/weight) primarily because all these variables are fundamentally directly related to the diameter of the lens. Synthetic aperture imaging provides a way to break away from these constraints by using a collection of sub-apertures. In the optical regime, these methods have not substantially impacted achievable performance thus far, but meta-optics offer a path to exploit this approach further.

The first examples of such synthetic aperture imaging using meta-surfaces have been in lower-frequency radar systems [153], utilizing dynamic metasurface antennas to generate tailored electromagnetic waveforms, achieving stripmap and spotlight synthetic aperture radar imaging. The use of metasurface antennas eliminates the need for mechanical gimbals and phase shifters,

simplifying the hardware architecture of a synthetic aperture system.

More recently, these techniques have been adapted to higher-frequency visible, infrared, and thermal imaging scenarios. Xu *et al*. [154] demonstrated a polarization-independent all-dielectric multifoci metalens by spatially integrating single-foci optical sparse-aperture sub-metalenses. Such a design allows the system to attain multiple focal points while retaining spatial resolution and other imaging characteristics comparable to a single-foci system [Figs. 7(a)–7(c)]. Zhao *et al*. [155] demonstrated that a synthetic aperture metalens composed of multiple metalenses with a relatively small aperture size can achieve an imaging resolution comparable to a conventional lens with an equivalent large aperture [Fig. 7(d)], validated via outdoor imaging using natural sunlight for target illumination.

These emerging approaches are only scratching the surface, and the potential for positive disruption based on these emerging synthetic aperture metalenses is quite encouraging. We would finally be able to break free from some of Lohman's scaling laws [156] for optical systems, and that would be transformative. Additionally, the synthetic aperture concept can potentially allow creating extremely large aperture optics, applicable for long-range imaging and laser-based space communications. Importantly, in such large systems, meta-optics can provide a significant weight advantage compared to bulky refractive optics.

C. Fourier Ptychography

Optical imaging systems are conventionally separated into incoherent and coherent systems. Incoherent systems form physical images using lenses and assume that field points are uncorrelated. Coherent systems use holography or phase retrieval and assume that all field points can interfere. Fourier ptychography (FP) may be viewed as an intermediary solution between these two extremes that combines focal processing to simplify and regularize the computational problem, but that also enables coherent wavefront reconstruction. FP has much less stringent coherence requirements than holography, enabling interferometric imaging with incoherent light-emitting diodes [157,158]. FP achieves coded irradiance oversampling by shifting the passband of imaging systems due to changes in the illumination pattern or imager perspective. A common approach is to shift the position of the capture lens in increments of $A/4$, where A is the aperture diameter. Unfortunately, this approach requires scanning with conventional optics, which makes snapshot imaging impossible. Meta-optics uniquely enable phase-diverse measurement from lenses with overlapping apertures, which enables snapshot Fourier ptychography. Such overlapping meta-lenslet arrays are possible due to the sub-wavelength periodicity of meta-optics, and as such very difficult, if not impossible, to realize using refractive or traditional diffractive optics. While the overlapping region is expected to suffer from lower transmission efficiency, the computational backend can be modified to overcome this issue, as demonstrated by others [116]. For coherent imaging applications, meta-optics are well suited given their chromatic sensitivity. The design and utility of meta-optics for coherent imaging are still preliminary, but early results suggest that meta-optics may enable a new category of imaging systems. For example, it is routine to make meta-optics operating at f/1, and using an array, it is possible to create systems operating with f/# well below 1, which enables high-resolution thin imagers. The optimal coding strategy and appropriate array design to enable such a thin camera will be a fascinating area of research.

D. High-Dynamic-Range Imaging

High-dynamic-range (HDR) imaging is essential for a wide range of applications in uncontrolled environments, including autonomous driving, robotics, and mobile phone cameras. Currently, the

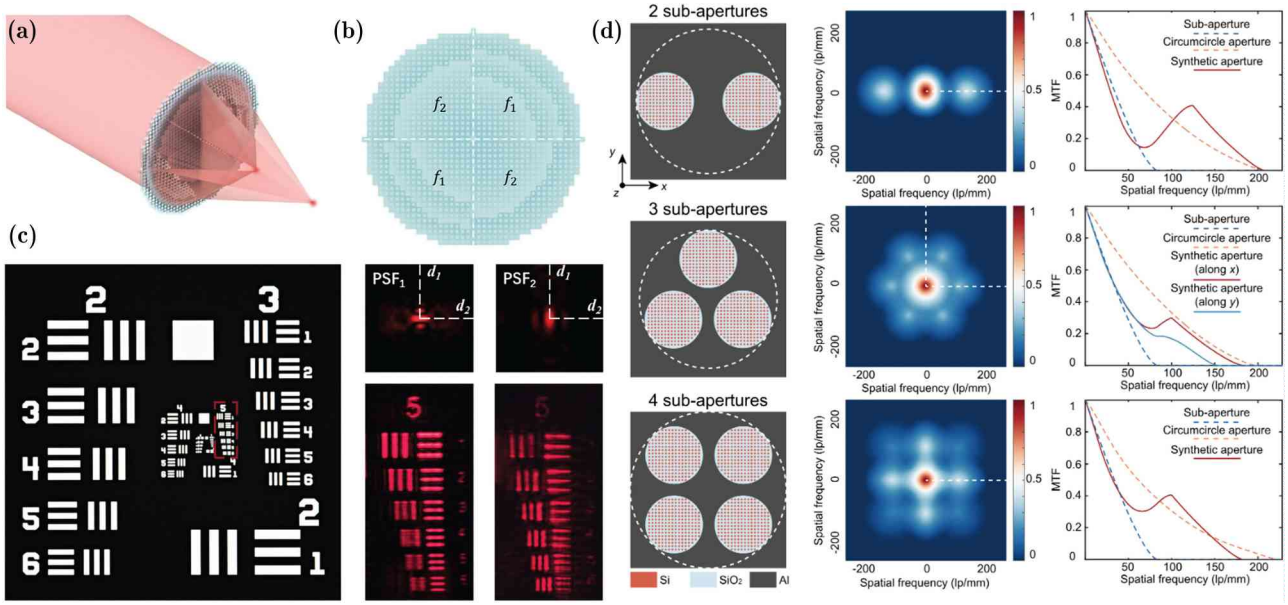

Fig. 7. (a) Schematic illustration of a multifocal sparse aperture metalens [154]. (b) Schematic of the all-dielectric MSA metalens with two focal points, $f_1 = 0.5$ mm and $f_2 = 1.0$ mm, respectively [154]. (c) Experimentally captured image of the USAF test target using the multifocal sparse aperture metalens at $\lambda = 650$ nm. (a)–(c) are reprinted with permission from Ref. [154] under Creative Commons Attribution license. (d) (left) Examples of three different sparse aperture array configurations, (middle) their corresponding two-dimensional MTFs, and (right) 1D plot lines of the MTFs (corresponding to dashed white lines in middle). Reprinted with permission from Ref. [155]. Copyright 2021 Optica Publishing Group.

dynamic range of a camera is limited by the sensor well capacity, fundamentally limiting conventional CMOS image sensors to a dynamic range of around ∼60–70 dB. Conventional sensors are unable to simultaneously capture a bright and a dark region outside of the sensor dynamic range in a single image, resulting in saturated bright regions or low SNR in dark regions. A large body of work explores different computational approaches to tackle these challenges. Traditionally, multiple low-dynamic-range (LDR) images are captured with different exposures to be combined into an HDR image [159,160]. Deep learning networks [161–163] have been used to generate plausible HDR content from a single LDR image based on imaging priors but are prone to hallucinating content and fail to recover saturated details faithfully.

Several works [164–166] proposed to distribute the otherwise saturated information into unsaturated regions, aiming primarily to recover small, saturated regions (3+ exposure value (EV)) in night-time photography. Applying reconfigurable meta-optics in this application could enable further improvements as well. Additionally, arrays of meta-optics, as recently explored for wide field-of-view broadband imaging [85], promise a new direction for HDR imaging. An immediate extension of existing methods [165] could employ an array of optical encodings tailored to several luminance bands spanning the target dynamic range. Further, co-designing these array elements along with temporal observations might offer fundamentally new insights. Here, the array elements could be learned to collaboratively cover the broadband spectrum and dynamic range, combining the capabilities of existing metasurfaces for capturing narrow spectral regions along with optical encodings that map saturated regions to unsaturated nearby spectral or spatial regions. Relying on temporal observations further increases the design space of this direction: in the form of a short or long burst, or exposure-bracketed acquisition along with the optical array encoding, which potentially could also be reconfigured per capture with reconfigurable metasurfaces.

E. Co-Optimized Meta-Optics with Sensors

Almost all existing computational cameras that rely on optical encodings have to solve a challenging inverse reconstruction problem for image recovery—they have to recover scene information that is encoded into the sensor measurements. Combining dual-pixel sensors with optical encodings that split the aperture into two halves could potentially allow us to simplify this problem by capturing two images simultaneously: one which applies an application-specific modulation to the incident light via a coded optical element to produce a coded image capture, and one that applies no modulation to produce a conventional image capture [167,168]. With such an uncoded conventional image as privileged information alongside the optically coded image in hand, we could investigate image reconstruction methods that are conditioned on the conventional image, making it possible to eliminate artifacts and compute costs that existing methods struggle with. Moreover, co-designing pixel circuitry on the sensor together with optics is an exciting direction for research. Co-designed spectrally sensitive dual-gain sensors with reconfigurable temporally switchable metasurfaces may offer insights into an exciting hybrid design space. Specifically, designing the spectral sensitivity of individual pixel sites jointly with metasurface optics, which are inherently diffractive, may allow for novel ways of spatially multiplexed measurements and hence improved spectral resolution [169] and dynamic range without giving up substantial spatial resolution. Together with temporal multiplexing, which switchable metasurfaces could enable, hybrid cameras allow for multispectral, full-dynamic-range cameras without the loss of any resolution.

While traditional sensors can be employed for such applications, a more intriguing direction will be to co-design pixel circuitry with the optics. Co-designed spectrally sensitive dual-gain sensors with reconfigurable temporally switchable metasurfaces may offer insights into an exciting hybrid design space. Recently, researchers reported human vision-inspired sensors to perform dual functionality: a cognition-oriented pathway for accurate cognition and an action-oriented pathway for rapid response [170]. Integrating such sensors with multifunctional meta-optics for foveated imaging [171] could provide true human-like vision. Integration of meta-optics with event cameras [172] can also provide ultra-low-power sensing. For example, several works exist on meta-optics-based edge detection [173,174]. However, from a system level, such edge detection provides little benefit in terms of power consumption, as we need to read out all the pixels in a conventional sensor. An event camera, on the other hand, only reads out changes in pixel intensities, substantially reducing energy consumption. As such, end-to-end design of the meta-optics, sensors, and computational backend will enable new sensing and imaging modalities and constitute a fertile research direction.

5. DISCUSSION

Current research on meta-optical computational imaging is primarily focused on full-color imaging, multimodal imaging (spectral and depth), and optical encoding for computer vision. While the field has progressed and the performance of the systems has improved dramatically, almost all demonstrations still lack the performance (in terms of resolution or accuracy) that can be achieved using state-of-the-art systems. While meta-optics can reduce size and weight, it remains unclear whether the performance degradation is acceptable. Hence, along with improving the performance, it is imperative to find applications where the pros of size reduction outweigh the cons of performance degradation. Two such applications could be endoscopy/angioscopy and also space-based imaging. While the first one requires an ultra-small aperture, the second one requires an extremely large aperture. As the field matures and advances in both computation and nanofabrication, a number of startups have begun commercializing meta-optics. Given the degrees of freedom offered by meta-optics, we anticipate this field to continue to grow and expect computational imaging to offer a pathway for mitigating some of the key challenges encountered by existing meta-optics.

Funding. Defense Advanced Research Projects Agency (W31P4Q21C0043); National Science Foundation (NSF-2127235).

Disclosures. Arka Majumdar is the co-founder of the startup Tunoptix, which is commercializing related technology.

Data availability. Data underlying the results presented in this paper are not publicly available at this time but may be obtained from the authors upon reasonable request.

Supplemental document. See Supplement 1 for supporting content.

REFERENCES

1. T. Ryhänen, M. A. Uusitalo, O. Ikkala, *et al.*, *Nanotechnologies for Future Mobile Devices* (Cambridge University, 2010).

2. L. E. Savastano, Q. Zhou, A. Smith, *et al.*, "Multimodal laser-based angioscopy for structural, chemical and biological imaging of atherosclerosis," Nat. Biomed. Eng. **1**, 0023 (2017).
3. L. E. Savastano and E. J. Seibel, "Scanning fiber angioscopy: a multimodal intravascular imaging platform for carotid atherosclerosis," Neurosurgery **64**, 188–198 (2017).
4. T. Stone and N. George, "Hybrid diffractive-refractive lenses and achromats," Appl. Opt. **27**, 2960–2971 (1988).
5. M. Kamali Seyedeh, E. Arbabi, A. Arbabi, *et al.*, "A review of dielectric optical metasurfaces for wavefront control," Nanophotonics **7**, 1041–1068 (2018).
6. P. Lalanne, S. Astilean, P. Chavel, *et al.*, "Design and fabrication of blazed binary diffractive elements with sampling periods smaller than the structural cutoff," J. Opt. Soc. Am. A **16**, 1143–1156 (1999).
7. S. Astilean, P. Lalanne, P. Chavel, *et al.*, "High-efficiency subwavelength diffractive element patterned in a high-refractive-index material for 633 nm," Opt. Lett. **23**, 552–554 (1998).
8. M. Delbracio, D. Kelly, M. S. Brown, *et al.*, "Mobile computational photography: a tour," Annu. Rev. Vision Sci. **7**, 571–604 (2021).
9. J. N. Mait, G. W. Euliss, and R. A. Athale, "Computational imaging," Adv. Opt. Photonics **10**, 409–483 (2018).
10. E. R. Dowski and W. T. Cathey, "Extended depth of field through wavefront coding," Appl. Opt. **34**, 1859–1866 (1995).
11. W. T. Cathey and E. R. Dowski, "New paradigm for imaging systems," Appl. Opt. **41**, 6080–6092 (2002).
12. P. R. Gill and D. G. Stork, "Lensless ultra-miniature imagers using odd-symmetry spiral phase gratings," in *Imaging and Applied Optics*, OSA Technical Digest (online) (Optical Society of America, 2013), paper CW4C.3.
13. P. Gill, *Enabling a Computer to Do the Job of a Lens* (SPIE, 2013).
14. E. L. Erickson, M. D. Kellam, P. R. Gill, *et al.*, "Miniature lensless computational infrared imager," Electron. Imaging **28**, 1–4 (2016).
15. F. Heide, M. Rouf, M. B. Hullin, *et al.*, "High-quality computational imaging through simple lenses," ACM Trans. Graph. **32**, 1–14 (2013).
16. M. A. Neifeld and P. Shankar, "Feature-specific imaging," Appl. Opt. **42**, 3379–3389 (2003).
17. C. Xia, J. Zhao, H. Cui, *et al.*, "DNNTune: automatic benchmarking DNN models for mobile-cloud computing," ACM Trans. Archit. Code Optim. **16**, 49 (2019).
18. L. Guolan and F. Baowei, "Medical hyperspectral imaging: a review," J. Biomed. Opt. **19**, 010901 (2014).
19. D.-W. Sun, H. Pu, and J. Yu, "Applications of hyperspectral imaging technology in the food industry," Nat. Rev. Electr. Eng. **1**, 251–263 (2024).
20. S. Zhou, T. Zhu, K. Shi, *et al.*, "Review of light field technologies," Vis. Comput. Ind. Biomed. Art **4**, 29 (2021).
21. R. Guo, Q. Yang, A. S. Chang, *et al.*, "EventLFM: event camera integrated Fourier light field microscopy for ultrafast 3D imaging," Light Sci. Appl. **13**, 144 (2024).
22. L. Hu, S. Hu, W. Gong, *et al.*, "Learning-based Shack-Hartmann wavefront sensor for high-order aberration detection," Opt. Express **27**, 33504–33517 (2019).
23. D. Wang, J. Song, J. Gao, *et al.*, "Computational polarization imaging in vivo through surgical smoke using refined polarization difference," Adv. Sci. **11**, 2309998 (2024).
24. J. N. Mait, R. A. Athale, J. van der Gracht, *et al.*, "Exploiting metamaterial characteristics for computational imaging," in *OSA Optical Design and Fabrication 2021 (Flat Optics, Freeform, IODC, OFT)*, OSA Technical Digest (Optica Publishing Group, 2021), paper FW5B.5.
25. J. Engelberg and U. Levy, "The advantages of metalenses over diffractive lenses," Nat. Commun. **11**, 1991 (2020).
26. S. Banerji, M. Meem, A. Majumder, *et al.*, "Imaging with flat optics: metalenses or diffractive lenses?" Optica **6**, 805–810 (2019).
27. A. Wirth-Singh, A. M. Jimenez, M. Choi, *et al.*, "Meta-optics triplet for zoom imaging at mid-wave infrared," Appl. Phys. Lett. **125**, 211705 (2024).
28. V. Liu and S. Fan, "S4: a free electromagnetic solver for layered periodic structures," Comput. Phys. Commun. **183**, 2233–2244 (2012).
29. F. Aieta, P. Genevet, M. A. Kats, *et al.*, "Aberration-free ultrathin flat lenses and axicons at telecom wavelengths based on plasmonic metasurfaces," Nano Lett. **12**, 4932–4936 (2012).
30. M. Khorasaninejad, W. T. Chen, R. C. Devlin, *et al.*, "Metalenses at visible wavelengths: diffraction-limited focusing and subwavelength resolution imaging," Science **352**, 1190 (2016).
31. A. Arbabi, Y. Horie, A. J. Ball, *et al.*, "Subwavelength-thick lenses with high numerical apertures and large efficiency based on high-contrast transmitarrays," Nat. Commun. **6**, 7069 (2015).
32. A. Zhan, S. Colburn, R. Trivedi, *et al.*, "Low-contrast dielectric metasurface optics," ACS Photonics **3**, 209–214 (2016).
33. M. Pu, X. Li, Y. Guo, *et al.*, "Nanoapertures with ordered rotations: symmetry transformation and wide-angle flat lensing," Opt. Express **25**, 31471–31477 (2017).
34. A. Martins, K. Li, J. Li, *et al.*, "On metalenses with arbitrarily wide field of view," ACS Photonics **7**, 2073–2079 (2020).
35. F. Yang, M. Shalaginov, H.-I. Lin, *et al.*, "Wide field-of-view metalens: a tutorial," Adv. Photonics **5**, 033001 (2023).
36. L. Huang, J. Whitehead, S. Colburn, *et al.*, "Design and analysis of extended depth of focus metalenses for achromatic computational imaging," Photonics Res. **8**, 1613–1623 (2020).
37. S. Colburn, A. Zhan, and A. Majumdar, "Metasurface optics for full-color computational imaging," Sci. Adv. **4**, eaar2114 (2018).
38. N. Yu, P. Genevet, M. A. Kats, *et al.*, "Light propagation with phase discontinuities: generalized laws of reflection and refraction," Science **334**, 333–337 (2011).
39. Y. Yang, W. Wang, P. Moitra, *et al.*, "Dielectric meta-reflectarray for broadband linear polarization conversion and optical vortex generation," Nano Lett. **14**, 1394–1399 (2014).
40. H. Ahmed, H. Kim, Y. Zhang, *et al.*, "Optical metasurfaces for generating and manipulating optical vortex beams," Nanophotonics **11**, 941–956 (2022).
41. M. Faraji-Dana, E. Arbabi, A. Arbabi, *et al.*, "Compact folded metasurface spectrometer," Nat. Commun. **9**, 4196 (2018).
42. J. E. Fröch, S. Colburn, A. Zhan, *et al.*, "Dual band computational infrared spectroscopy via large aperture meta-optics," ACS Photonics **10**, 986–992 (2022).
43. A. Y. Zhu, W.-T. Chen, M. Khorasaninejad, *et al.*, "Ultra-compact visible chiral spectrometer with meta-lenses," APL Photonics **2**, 036103 (2017).
44. N. A. Rubin, G. D'Aversa, P. Chevalier, *et al.*, "Matrix Fourier optics enables a compact full-Stokes polarization camera," Science **365**, eaax1839 (2019).
45. Z. Yang, Z. Wang, Y. Wang, *et al.*, "Generalized Hartmann-Shack array of dielectric metalens sub-arrays for polarimetric beam profiling," Nat. Commun. **9**, 4607 (2018).
46. C. Ogawa, S. Nakamura, T. Aso, *et al.*, "Rotational varifocal moiré metalens made of single-crystal silicon meta-atoms for visible wavelengths," Nanophotonics **11**, 1941–1948 (2022).
47. Z. Liu, Z. Du, B. Hu, *et al.*, "Wide-angle Moiré metalens with continuous zooming," J. Opt. Soc. Am. B **36**, 2810–2816 (2019).
48. Y. Luo, C. H. Chu, S. Vyas, *et al.*, "Varifocal metalens for optical sectioning fluorescence microscopy," Nano Lett. **21**, 5133–5142 (2021).
49. A. Zhan, S. Colburn, C. M. Dodson, *et al.*, "Metasurface freeform nanophotonics," Sci. Rep. **7**, 1673 (2017).
50. S. Colburn, A. Zhan, and A. Majumdar, "Varifocal zoom imaging with large area focal length adjustable metalenses," Optica **5**, 825–831 (2018).
51. S. Colburn and A. Majumdar, "Metasurface generation of paired accelerating and rotating optical beams for passive ranging and scene reconstruction," ACS Photonics **7**, 1529–1536 (2020).
52. Z. Shen, F. Zhao, C. Jin, *et al.*, "Monocular metasurface camera for passive single-shot 4D imaging," Nat. Commun. **14**, 1035 (2023).
53. D. K. Sharma, K. H. Lai, A. V. Baranikov, *et al.*, "Stereo imaging with a hemispherical field-of-view metalens camera," ACS Photonics **11**, 2016–2021 (2024).
54. R. Pestourie, C. Pérez-Arancibia, Z. Lin, *et al.*, "Inverse design of large-area metasurfaces," Opt. Express **26**, 33732–33747 (2018).
55. C. Pérez-Arancibia, R. Pestourie, and S. G. Johnson, "Sideways adiabaticity: beyond ray optics for slowly varying metasurfaces," Opt. Express **26**, 30202–30230 (2018).
56. Z. Lin and S. G. Johnson, "Overlapping domains for topology optimization of large-area metasurfaces," Opt. Express **27**, 32445–32453 (2019).
57. M. Zhelyeznyakov, J. Fröch, A. Wirth-Singh, *et al.*, "Large area optimization of meta-lens via data-free machine learning," Commun. Eng. **2**, 60 (2023).
58. V. Egede Johansen, U. M. Gür, J. Martínez-Llinás, *et al.*, "Nanoscale precision brings experimental metalens efficiencies on par with theoretical promises," Commun. Phys. **7**, 123 (2024).

59. J. Engelberg and U. Levy, "Achromatic flat lens performance limits," Optica **8**, 834–845 (2021).
60. A. Wirth-Singh, J. E. Fröch, F. Yang, *et al.*, "Wide field of view large aperture meta-doublet eyepiece," arXiv, (2024).
61. E. Arbabi, A. Arbabi, S. M. Kamali, *et al.*, "Multiwavelength polarization-insensitive lenses based on dielectric metasurfaces with meta-molecules," Optica **3**, 628–633 (2016).
62. Z. Shi, M. Khorasaninejad, Y.-W. Huang, *et al.*, "Single-layer metasurface with controllable multiwavelength functions," Nano Lett. **18**, 2420–2427 (2018).
63. L. Huang, S. Colburn, A. Zhan, *et al.*, "Full-color metaoptical imaging in visible light," Adv. Photonics Res. **3**, 2100265 (2022).
64. W. T. Chen, A. Y. Zhu, V. Sanjeev, *et al.*, "A broadband achromatic metalens for focusing and imaging in the visible," Nat. Nanotechnol. **13**, 220–226 (2018).
65. S. Shrestha, A. C. Overvig, M. Lu, *et al.*, "Broadband achromatic dielectric metalenses," Light Sci. Appl. **7**, 85 (2018).
66. S. Wang, P. C. Wu, V.-C. Su, *et al.*, "A broadband achromatic metalens in the visible," Nat. Nanotechnol. **13**, 227–232 (2018).
67. W. T. Chen, A. Y. Zhu, J. Sisler, *et al.*, "A broadband achromatic polarization-insensitive metalens consisting of anisotropic nanostructures," Nat. Commun. **10**, 355 (2019).
68. F. Balli, M. Sultan, S. K. Lami, *et al.*, "A hybrid achromatic metalens," Nat. Commun. **11**, 3892 (2020).
69. A. Ndao, L. Hsu, J. Ha, *et al.*, "Octave bandwidth photonics fishnet-achromatic-metalens," Nat. Commun. **11**, 3205 (2020).
70. Y. Hu, Y. Jiang, Y. Zhang, *et al.*, "Asymptotic dispersion engineering for ultra-broadband meta-optics," Nat. Commun. **14**, 6649 (2023).
71. W. T. Chen, A. Y. Zhu, and F. Capasso, "Flat optics with dispersion-engineered metasurfaces," Nat. Rev. Mater. **5**, 604–620 (2020).
72. F. Presutti and F. Monticone, "Focusing on bandwidth: achromatic metalens limits," Optica **7**, 624–631 (2020).
73. Z. Li, R. Pestourie, Z. Lin, *et al.*, "Empowering metasurfaces with inverse design: principles and applications," ACS Photonics **9**, 2178–2192 (2022).
74. R. W. Gerchberg, "A practical algorithm for the determination of phase from image and diffraction plane pictures," Optik **35**, 237–246 (1972).
75. E. Tseng, S. Colburn, J. Whitehead, *et al.*, "Neural nano-optics for high-quality thin lens imaging," Nat. Commun. **12**, 6493 (2021).
76. Z. Li, R. Pestourie, J.-S. Park, *et al.*, "Inverse design enables large-scale high-performance meta-optics reshaping virtual reality," Nat. Commun. **13**, 2409 (2022).
77. A. Sinha, J. Lee, S. Li, *et al.*, "Lensless computational imaging through deep learning," Optica **4**, 1117–1125 (2017).
78. G. Kim and R. Menon, "Computational imaging enables a "see-through" lens-less camera," Opt. Express **26**, 22826–22836 (2018).
79. A. Ozcan and E. McLeod, "Lensless imaging and sensing," Annu. Rev. Biomed. Eng. **18**, 77–102 (2016).
80. O. S. Cossairt, D. Miau, and S. K. Nayar, "Gigapixel computational imaging," in *IEEE International Conference on Computational Photography (ICCP)* (2011), pp. 1–8.
81. N. Antipa, G. Kuo, R. Heckel, *et al.*, "DiffuserCam: lensless single-exposure 3D imaging," Optica **5**, 1–9 (2018).
82. M. S. Asif, A. Ayremlou, A. Sankaranarayanan, *et al.*, "FlatCam: thin, lensless cameras using coded aperture and computation," IEEE Trans. Comput. Imaging **3**, 384–397 (2017).
83. J. Suo, W. Zhang, J. Gong, *et al.*, "Computational imaging and artificial intelligence: the next revolution of mobile vision," Proc. IEEE **111**, 1607–1639 (2023).
84. Y. Dong, B. Zheng, H. Li, *et al.*, "Achromatic single metalens imaging via deep neural network," ACS Photonics **11**, 1645–1656 (2024).
85. P. Chakravarthula, J. Sun, X. Li, *et al.*, "Thin on-sensor nanophotonics array cameras," ACM Trans. Graph. **42**, 249 (2023).
86. J. Yeo, D. Loh, R. Paniagua-Dominguez, *et al.*, "EigenCWD: a spatially-varying deconvolution algorithm for single metalens imaging," arXiv, (2025).
87. S. Dong, R. Horstmeyer, R. Shiradkar, *et al.*, "Aperture-scanning Fourier ptychography for 3D refocusing and super-resolution macroscopic imaging," Opt. Express **22**, 13586–13599 (2014).
88. R. Heintzmann and M. G. L. Gustafsson, "Subdiffraction resolution in continuous samples," Nat. Photonics **3**, 362–364 (2009).
89. K. Yanny, N. Antipa, W. Liberti, *et al.*, "Miniscope3D: optimized single-shot miniature 3D fluorescence microscopy," Light Sci. Appl. **9**, 171 (2020).
90. A. Greengard, Y. Y. Schechner, and R. Piestun, "Depth from diffracted rotation," Opt. Lett. **31**, 181–183 (2006).
91. S. R. P. Pavani, M. A. Thompson, J. S. Biteen, *et al.*, "Three-dimensional, single-molecule fluorescence imaging beyond the diffraction limit by using a double-helix point spread function," Proc. Natl. Acad. Sci. USA **106**, 2995–2999 (2009).
92. D. J. Brady, M. E. Gehm, R. A. Stack, *et al.*, "Multiscale gigapixel photography," Nature **486**, 386–389 (2012).
93. E. Arbabi, A. Arbabi, S. M. Kamali, *et al.*, "Controlling the sign of chromatic dispersion in diffractive optics with dielectric metasurfaces," Optica **4**, 625–632 (2017).
94. M. Khorasaninejad, Z. Shi, A. Y. Zhu, *et al.*, "Achromatic metalens over 60 nm bandwidth in the visible and metalens with reverse chromatic dispersion," Nano Lett. **17**, 1819–1824 (2017).
95. S. Wang, P. C. Wu, V.-C. Su, *et al.*, "Broadband achromatic optical metasurface devices," Nat. Commun. **8**, 187 (2017).
96. W. Chi and N. George, "Electronic imaging using a logarithmic asphere," Opt. Lett. **26**, 875–877 (2001).
97. E. Bayati, R. Pestourie, S. Colburn, *et al.*, "Inverse designed extended depth of focus meta-optics for broadband imaging in the visible," Nanophotonics **11**, 2531–2540 (2022).
98. L. Huang, Z. Han, A. Wirth-Singh, *et al.*, "Broadband thermal imaging using meta-optics," Nat. Commun. **15**, 1662 (2024).
99. F. Yang, S. An, M. Y. Shalaginov, *et al.*, "Design of broadband and wide-field-of-view metalenses," Opt. Lett. **46**, 5735–5738 (2021).
100. J. E. Fröch, P. K. Chakravarthula, J. Sun, *et al.*, "Beating spectral bandwidth limits for large aperture broadband nano-optics," Nat Commun **16**, 3025 (2025).
101. R. Maman, E. Mualem, N. Mazurski, *et al.*, "Achromatic imaging systems with flat lenses enabled by deep learning," ACS Photonics **10**, 4494–4500 (2023).
102. W. T. Chen, A. Y. Zhu, J. Sisler, *et al.*, "Broadband achromatic metasurface-refractive optics," Nano Lett. **18**, 7801–7808 (2018).
103. S. Pinilla, J. E. Fröch, S. R. Miri Rostami, *et al.*, "Miniature color camera via flat hybrid meta-optics," Sci. Adv. **9**, eadg7297 (2023).
104. M. Faraji-Dana, E. Arbabi, H. Kwon, *et al.*, "Hyperspectral imager with folded metasurface optics," ACS Photonics **6**, 2161–2167 (2019).
105. A. McClung, S. Samudrala, M. Torfeh, *et al.*, "Snapshot spectral imaging with parallel metasystems," Sci. Adv. **6**, eabc7646 (2020).
106. H. Arguello, S. Pinilla, Y. Peng, *et al.*, "Shift-variant color-coded diffractive spectral imaging system," Optica **8**, 1424–1434 (2021).
107. S. R. P. Pavani and R. Piestun, "Three dimensional tracking of fluorescent microparticles using a photonics-limited double-helix response system," Opt. Express **16**, 22048–22057 (2008).
108. M. Badieirostami, M. D. Lew, M. A. Thompson, *et al.*, "Three-dimensional localization precision of the double-helix point spread function versus astigmatism and biplane," Appl. Phys. Lett. **97**, 161103 (2010).
109. M. A. Thompson, M. D. Lew, M. Badieirostami, *et al.*, "Localizing and tracking single nanoscale emitters in three dimensions with high spatiotemporal resolution using a double-helix point spread function," Nano Lett. **10**, 211–218 (2010).
110. S. Quirin and R. Piestun, "Depth estimation and image recovery using broadband, incoherent illumination with engineered point spread functions [Invited]," Appl. Opt. **52**, A367–A376 (2013).
111. F. Yang, H.-I. Lin, P. Chen, *et al.*, "Monocular depth sensing using metalens," Nanophotonics **12**, 2987–2996 (2023).
112. Q. Guo, Z. Shi, Y.-W. Huang, *et al.*, "Compact single-shot metalens depth sensors inspired by eyes of jumping spiders," Proc. Natl. Acad. Sci. USA **116**, 22959–22965 (2019).
113. https://creativecommons.org/licenses/by/4.0/.
114. A. Shanker, J. Froech, S. Mukherjee, *et al.*, "Quantitative phase imaging with a metalens," arXiv, (2024).
115. R. J. Lin, V.-C. Su, S. Wang, *et al.*, "Achromatic metalens array for full-colour light-field imaging," Nat. Nanotechnol. **14**, 227–231 (2019).
116. A. L. Holsteen, D. Lin, I. Kauvar, *et al.*, "A light-field metasurface for high-resolution single-particle tracking," Nano Lett. **19**, 2267–2271 (2019).
117. J. E. M. Whitehead, A. Zhan, S. Colburn, *et al.*, "Fast extended depth of focus meta-optics for varifocal functionality," Photonics Res. **10**, 828–833 (2022).

118. C.-C. Tsai, X. Huang, Z. Wu, *et al.*, "Metasurface smart glass for object recognition," arXiv, (2022).
119. T. Wang, S. Y. Ma, L. G. Wright, *et al.*, "An optical neural network using less than 1 photonics per multiplication," Nat. Commun. **13**, 123 (2022).
120. H. Zheng, Q. Liu, Y. Zhou, *et al.*, "Meta-optic accelerators for object classifiers," Sci. Adv. **8**, eabo6410 (2022).
121. S. Colburn, Y. Chu, E. Shilzerman, *et al.*, "Optical frontend for a convolutional neural network," Appl. Opt. **58**, 3179–3186 (2019).
122. X. Lin, Y. Rivenson, N. T. Yardimci, *et al.*, "All-optical machine learning using diffractive deep neural networks," Science **361**, 1004–1008 (2018).
123. L. Huang, Q. A. A. Tanguy, J. E. Fröch, *et al.*, "Photonics advantage of optical encoders," Nanophotonics **13**, 1191–1196 (2023).
124. K. Wei, X. Li, J. Froech, *et al.*, "Spatially varying nanophotonics neural networks," arXiv, (2023).
125. J. N. Mait and W. T. Rhodes, "Pupil function design algorithm for bipolar incoherent spatial filtering," Appl. Opt. **28**, 1474–1488 (1989).
126. J. Xiang, S. Colburn, A. Majumdar, *et al.*, "Knowledge distillation circumvents nonlinearity for optical convolutional neural networks," Appl. Opt. **61**, 2173–2183 (2022).
127. A. Wirth-Singh, J. Xiang, M. Choi, *et al.*, "Compressed meta-optical encoder for image classification," arXiv, (2024).
128. K. Wei, X. Li, J. Froech, *et al.*, "Spatially varying nanophotonics neural networks," Sci. Adv. **10**, eadp0391 (2024).
129. C. M. V. Burgos, T. Yang, Y. Zhu, *et al.*, "Design framework for metasurface optics-based convolutional neural networks," Appl. Opt. **60**, 4356–4365 (2021).
130. M. Choi, J. Xiang, A. Wirth-Singh, *et al.*, "Transferable polychromatic optical encoder for neural networks," arXiv, (2024).
131. H. Zheng, Q. Liu, I. I. Kravchenko, *et al.*, "Multichannel meta-imagers for accelerating machine vision," Nat. Nanotechnol. **19**, 471–478 (2024).
132. A. Dosovitskiy, L. Beyer, A. Kolesnikov, *et al.*, "An image is worth 16x16 words: transformers for image recognition at scale," arXiv, (2020).
133. A. H. Dorrah and F. Capasso, "Tunable structured light with flat optics," Science **376**, eabi6860 (2022).
134. Q. He, S. Sun, and L. Zhou, "Tunable/reconfigurable metasurfaces: physics and applications," Research **2019**, 1849272 (2019).
135. J. Park, B. G. Jeong, S. I. Kim, *et al.*, "All-solid-state spatial light modulator with independent phase and amplitude control for three-dimensional LiDAR applications," Nat. Nanotechnol. **16**, 69–76 (2021).
136. G. K. Shirmanesh, R. Sokhoyan, P. C. Wu, *et al.*, "Electro-optically tunable multifunctional metasurfaces," ACS Nano **14**, 6912–6920 (2020).
137. I.-C. Benea-Chelmus, M. L. Meretska, D. L. Elder, *et al.*, "Electro-optic spatial light modulator from an engineered organic layer," Nat. Commun. **12**, 5928 (2021).
138. R. Chen, V. Tara, A.-W. Singh, *et al.*, "A hybrid solution for spatial light modulators with a large space-bandwidth product: opinion," Opt. Mater. Express **13**, 2416–2421 (2023).
139. S.-Q. Li, X. Xu, R. Maruthiyodan Veetil, *et al.*, "Phase-only transmissive spatial light modulator based on tunable dielectric metasurface," Science **364**, 1087–1090 (2019).
140. E. Arbabi, A. Arbabi, S. M. Kamali, *et al.*, "MEMS-tunable dielectric metasurface lens," Nat. Commun. **9**, 812 (2018).
141. Z. Han, S. Colburn, A. Majumdar, *et al.*, "MEMS-actuated metasurface Alvarez lens," Microsyst. Nanoeng. **6**, 79 (2020).
142. H. Kwon, T. Zheng, and A. Faraon, "Nano-electromechanical spatial light modulator enabled by asymmetric resonant dielectric metasurfaces," Nat. Commun. **13**, 5811 (2022).
143. P. Moitra, X. Xu, R. Maruthiyodan Veetil, *et al.*, "Electrically tunable reflective metasurfaces with continuous and full-phase modulation for high-efficiency wavefront control at visible frequencies," ACS Nano **17**, 16952–16959 (2023).
144. H. Kwon, T. Zheng, and A. Faraon, "Nano-electromechanical tuning of dual-mode resonant dielectric metasurfaces for dynamic amplitude and phase modulation," Nano Lett. **21**, 2817–2823 (2021).
145. D. Bloom, "Grating light valve: revolutionizing display technology," Proc. SPIE **3013**, 165–171 (1997).
146. S. Abdollahramezani, O. Hemmatyar, H. Taghinejad, *et al.*, "Tunable nanophotonics enabled by chalcogenide phase-change materials," Nanophotonics **9**, 1189–1241 (2020).
147. Z. Fang, R. Chen, V. Tara, *et al.*, "Non-volatile phase-change materials for programmable photonics," Sci. Bull. **68**, 783–786 (2023).
148. Y. Zhang, C. Ríos, M. Y. Shalaginov, *et al.*, "Myths and truths about optical phase change materials: a perspective," Appl. Phys. Lett. **118**, 210501 (2021).
149. S. Abdollahramezani, O. Hemmatyar, M. Taghinejad, *et al.*, "Electrically driven reprogrammable phase-change metasurface reaching 80% efficiency," Nat. Commun. **13**, 1696 (2022).
150. M. Y. Shalaginov, S. An, Y. Zhang, *et al.*, "Reconfigurable all-dielectric metalens with diffraction-limited performance," Nat. Commun. **12**, 1225 (2021).
151. Y. Wang, P. Landreman, D. Schoen, *et al.*, "Electrical tuning of phase-change antennas and metasurfaces," Nat. Nanotechnol. **16**, 667–672 (2021).
152. Z. Fang, R. Chen, J. E. Fröch, *et al.*, "Nonvolatile phase-only transmissive spatial light modulator with electrical addressability of individual pixels," ACS Nano **18**, 11245–11256 (2024).
153. M. Boyarsky, T. Sleasman, L. Pulido-Mancera, *et al.*, "Synthetic aperture radar with dynamic metasurface antennas: a conceptual development," J. Opt. Soc. Am. A **34**, A22–A36 (2017).
154. B. Xu, W. Wei, P. Tang, *et al.*, "A multi-foci sparse-aperture metalens," Adv. Sci. **11**, 2309648 (2024).
155. F. Zhao, Z. Shen, D. Wang, *et al.*, "Synthetic aperture metalens," Photonics Res. **9**, 2388–2397 (2021).
156. A. W. Lohmann, "Scaling laws for lens systems," Appl. Opt. **28**, 4996–4998 (1989).
157. G. Zheng, C. Shen, S. Jiang, *et al.*, "Concept, implementations and applications of Fourier ptychography," Nat. Rev. Phys. **3**, 207–223 (2021).
158. P. C. Konda, L. Loetgering, K. C. Zhou, *et al.*, "Fourier ptychography: current applications and future promises," Opt. Express **28**, 9603–9630 (2020).
159. P. E. Debevec and J. Malik, "Recovering high dynamic range radiance maps from photographs," in *Seminal Graphics Papers: Pushing the Boundaries* (Association for Computing Machinery, 2023), Vol. **2**, p. 67.
160. E. Reinhard, G. Ward, S. Pattanaik, *et al.*, *High Dynamic Range Imaging: Acquisition, Display, and Image-Based Lighting*, The Morgan Kaufmann Series in Computer Graphics (Morgan Kaufmann, 2005).
161. S. K. Chen, H. L. Yen, Y. L. Liu, *et al.*, "Learning continuous exposure value representations for single-image HDR reconstruction," in *IEEE/CVF International Conference on Computer Vision (ICCV)* (2023), pp. 12944–12954.
162. Z. Khan, M. Khanna, and S. Raman, "FHDR: HDR image reconstruction from a single LDR image using feedback network," in *IEEE Global Conference on Signal and Information Processing (GlobalSIP)* (2019), pp. 1–5.
163. M. S. Santos, T. I. Ren, and N. K. Kalantari, "Single image HDR reconstruction using a CNN with masked features and perceptual loss," ACM Trans. Graph. **39**, 80 (2020).
164. M. Rouf, R. Mantiuk, W. Heidrich, *et al.*, "Glare encoding of high dynamic range images," in *Conference on Computer Vision and Pattern Recognition* (2011), pp. 289–296.
165. Q. Sun, E. Tseng, Q. Fu, *et al.*, "Learning rank-1 diffractive optics for single-shot high dynamic range imaging," in *Proceedings of the IEEE/CVF Conference on Computer Vision and Pattern Recognition* (2020), pp. 1386–1396.
166. C. A. Metzler, H. Ikoma, Y. Peng, *et al.*, "Deep optics for single-shot high-dynamic-range imaging," in *IEEE/CVF Conference on Computer Vision and Pattern Recognition (CVPR)* (2020), pp. 1372–1382.
167. Z. Shi, I. Chugunov, M. Bijelic, *et al.*, "Split-aperture 2-in-1 computational cameras," ACM Trans. Graph. **43**, 141 (2024).
168. M. Aggarwal and N. Ahuja, "Split aperture imaging for high dynamic range," Int. J. Comput. Vis. **58**, 7–17 (2004).
169. Z. Shi, X. Dun, H. Wei, *et al.*, "Learned multi-aperture color-coded optics for snapshot hyperspectral imaging," ACM Trans. Graph. **43**, 208 (2024).
170. Z. Yang, T. Wang, Y. Lin, *et al.*, "A vision chip with complementary pathways for open-world sensing," Nature **629**, 1027–1033 (2024).
171. V. Saragadam, Z. Han, V. Boominathan, *et al.*, "Foveated thermal computational imaging prototype using all-silicon meta-optics," Optica **11**, 18–25 (2024).

172. D. Gehrig and D. Scaramuzza, "Low-latency automotive vision with event cameras," Nature **629**, 1034–1040 (2024).
173. Y. Zhou, H. Zheng, I. I. Kravchenko, *et al.*, "Flat optics for image differentiation," Nat. Photonics **14**, 316–323 (2020).
174. B. T. Swartz, H. Zheng, G. T. Forcherio, *et al.*, "Broadband and large-aperture metasurface edge encoders for incoherent infrared radiation," Sci. Adv. **10**, eadk0024 (2024).